MNRAS 000, 1–11 (2023) Preprint 9 March 2023 Compiled using MNRAS LaTeX style file v3.0

Multiwavelength observations of the extraordinary accretion event AT2021lwx

P. Wiseman,[1★] Y. Wang,[1], S. Hönig,[1], N. Castro-Segura,[1] P. Clark,[2] C. Frohmaier,[1] M. D. Fulton,[3] G. Leloudas,[4] M. Middleton,[1] T. E. Müller-Bravo,[5,6] A. Mummery,[7] M. Pursiainen,[4] S. J. Smartt,[7,3] K. Smith,[3] M. Sullivan,[1], J. P. Anderson,[8,9] J. A. Acosta Pulido,[10,11] P. Charalampopoulos,[12] M. Banerji,[1] M. Dennefeld,[13] L. Galbany,[5] M. Gromadzki,[14] C. P. Gutiérrez[15,16] N. Ihanec,[14] E. Kankare,[12,17] A. Lawrence,[18] B. Mockler,[19] T. Moore,[3] M. Nicholl,[3] F. Onori,[20] T. Petrushevska,[21] F. Ragosta,[22] S. Rest,[23] M. Smith,[24] T. Wevers,[8] R. Carini,[22] T.-W. Chen,[25,26] K. Chambers,[27] H. Gao,[27] M. Huber,[27] C. Inserra,[28] E. Magnier,[27] L. Makrygianni,[29] M. Toy,[1] F. Vincentelli,[10] D. R. Young,[3]

[1] School of Physics and Astronomy, University of Southampton, Southampton, SO17 1BJ, UK
[2] Institute of Cosmology and Gravitation, University of Portsmouth, Portsmouth, PO1 3FX, UK
[3] Astrophysics Research Centre, School of Mathematics and Physics, Queen's University Belfast, BT7 1NN, UK
[4] DTU Space, National Space Institute, Technical University of Denmark, Elektrovej 327, 2800 Kgs. Lyngby, Denmark
[5] Institute of Space Sciences (ICE, CSIC), Campus UAB, Carrer de Can Magrans, s/n, E-08193 Barcelona, Spain
[6] Institut d'Estudis Espacials de Catalunya (IEEC), E-08034 Barcelona, Spain
[7] Department of Physics, University of Oxford, Denys Wilkinson Building, Keble Road, Oxford OX1 3RH, UK
[8] European Southern Observatory, Alonso de Córdova 3107, Casilla 19, Santiago, Chile
[9] Millennium Institute of Astrophysics MAS, Nuncio Monsenor Sotero Sanz 100, Off. 104, Providencia, Santiago, Chile
[10] Instituto de Astrofísica de Canarias (IAC), E-38200 La Laguna, Tenerife, Spain
[11] Universidad de La Laguna (ULL), Departamento de Astrofisica, E-38206, Tenerife, Spain
[12] Department of Physics and Astronomy, University of Turku, FI-20014 Turku, Finland
[13] Institut d'Astrophysique de Paris (IAP), CNRS & Sorbonne Université, 75014 Paris, France
[14] Astronomical Observatory, University of Warsaw, Al. Ujazdowskie 4, 00-478 Warszawa, Poland
[15] Finnish Centre for Astronomy with ESO (FINCA), FI-20014 University of Turku, Finland
[16] Tuorla Observatory, Department of Physics and Astronomy, FI-20014 University of Turku, Finland
[17] Turku Collegium for Science, Medicine and Technology, University of Turku, FI-20014 Turku, Finland
[18] Institute for Astronomy, University of Edinburgh, Royal Observatory, Blackford Hill, Edinburgh EH9 3HJ
[19] Department of Astronomy and Astrophysics, University of California, Santa Cruz, Santa Cruz, CA 95064, USA
[20] INAF - Osservatorio Astronomico d'Abruzzo, Via M. Maggini snc, I-64100 Teramo, Italy
[21] University of Nova Gorica, Center for Astrophysics and Cosmology, Vipavska 11c, SI-5270 Ajdovščina, Slovenia
[22] INAF-Osservatorio Astronomico di Roma, via Frascati 33, 00078 Monte Porzio Catone (RM), Italy
[23] Department of Physics and Astronomy, The Johns Hopkins University, Baltimore, MD 21218, USA
[24] Univ Lyon, Univ Claude Bernard Lyon 1, CNRS, IP2I Lyon / IN2P3, IMR 5822, F-69622 Villeurbanne, France
[25] Technische Universität München, TUM School of Natural Sciences, Physik-Department, James-Franck-Straße 1, 85748 Garching, Germany
[26] Max-Planck-Institut für Astrophysik, Karl-Schwarzschild Straße 1, 85748 Garching, Germany [27] Institute for Astronomy, University of Hawaii, 2680 Woodlawn Drive, Hon
[28] Cardiff Hub for Astrophysics Research and Technology, School of Physics & Astronomy, Cardiff University, Queens Buildings, The Parade, Cardiff, CF24 3AA, UK
[29] The School of Physics and Astronomy, Tel Aviv University, Tel Aviv 69978, Israel

Accepted XXX. Received YYY; in original form ZZZ

ABSTRACT

We present observations from X-ray to mid-infrared wavelengths of the most energetic non-quasar transient ever observed, AT2021lwx. Our data show a single optical brightening by a factor > 100 to a luminosity of 7×10^{45} erg s^{-1}, and a total radiated energy of 1.5×10^{53} erg, both greater than any known optical transient. The decline is smooth and exponential and the ultra-violet - optical spectral energy distribution resembles a black body with temperature 1.2×10^4 K. Tentative X-ray detections indicate a secondary mode of emission, while a delayed mid-infrared flare points to the presence of dust surrounding the transient. The spectra are similar to recently discovered optical flares in known active galactic nuclei but lack some characteristic features. The lack of emission for the previous seven years is inconsistent with the short-term, stochastic variability observed in quasars, while the extreme luminosity and long timescale of the transient disfavour the disruption of a single solar-mass star. The luminosity could be generated by the disruption of a much more massive star, but the likelihood of such an event occurring is small. A plausible scenario is the accretion of a giant molecular cloud by a dormant black hole of $10^8 - 10^9$ solar masses. AT2021lwx thus represents an extreme extension of the known scenarios of black hole accretion.

Key words: accretion, accretion discs – transients: tidal disruption events – Transients – galaxies: active – quasars: supermassive black holes

1 INTRODUCTION

The accretion of matter onto supermassive black holes (SMBHs) is the most efficient known process of extracting energy in the Universe, with general relativistic effects combined with complex magneto-hydrodynamics and highly non-thermal radiative processes causing spectacular electromagnetic phenomena. This accretion can happen at a widely varying range of rates: steadily-accreting SMBHs, called active galactic nuclei (AGN), are the central engines of galaxies, which accrete gas for Myr at a time with a rate that typically varies on timescales of seconds to years (e.g. McHardy et al. 2006; Scaringi et al. 2015).

As opposed to typical variability of AGN caused by stochastic accretion, tidal disruption events (TDEs) represent a much shorter, yet far more violent accretion episode. These phenomena are caused by the destruction of a star in the vicinity of a SMBH (or intermediate-mass black hole; Angus et al. 2022) due to tidal forces. TDEs usually reveal themselves through a single flare observed in optical/ultraviolet (UV)/X-rays with a smooth rise and decaying light curve. Not all SMBHs are equally likely to produce a TDE: for SMBHs with masses $M_{\rm BH} \gtrsim 10^8\,{\rm M}_\odot$, the tidal radius of a solar mass star lies within the innermost stable circular orbit (ISCO) of the black hole, which suppresses or completely prohibits TDEs (the exact limit depends on stellar type and SMBH spin). Indeed, observed or model-inferred masses of TDEs suggest $M_{\rm BH} \sim 5\times10^5 - 10^7\,{\rm M}_\odot$ and $M_* \sim 0.6-13\,{\rm M}_\odot$ (Mockler et al. 2019; Ryu et al. 2020), though the high end of this stellar mass range is highly uncertain. TDEs display broad emission lines, often of hydrogen and/or helium, and many show ionised iron and Bowen flourescence lines of nitrogen and oxygen (e.g. Arcavi et al. 2014; Leloudas et al. 2019; van Velzen et al. 2021), indicative of the presence of a UV-bright accretion disk.

The clear differences between regular AGN variability and TDEs are muddied by the addition of recently-discovered changing look AGN (CLAGNs; LaMassa et al. 2015) and SMBH 're-ignitions' (Trakhtenbrot et al. 2019). CLAGNs tend to exhibit changes in their spectral properties such as line widths and continuum slopes (Komossa et al. 2022), sometimes accompanied by X-ray outbursts and a change in optical brightness but critically while maintaining their usual variable optical light curve. On the other hand, re-ignitions and flares appear as a single highly luminous optical transient (Kankare et al. 2017; Gromadzki et al. 2019; Trakhtenbrot et al. 2019; Frederick et al. 2021). The spectra of these flares, which are often found in narrow-line Seyfert 1 (NLSy1) host galaxies, show ubiquitous hydrogen Balmer emission lines as well as many of the same helium and Bowen features of TDEs (Frederick et al. 2021), although the line profiles (particularly of hydrogen) tend to be narrower. While the high luminosity of the flares necessitates a large amount of material being accreted, the exact nature remains a mystery, with various sources labelled as possible abnormal TDEs or sudden changes in the accretion flow of already-accreting SMBHs.

Here we present multiwavelength observations of AT2021lwx, the most luminous of such flares ever detected. AT2021lwx, at z = 0.9945, displays properties spanning TDEs, SMBH flares, and AGN, while unlike all of those classes there is no host galaxy visible to deep limits in pre-outburst survey data. Our observations (Section 2) span nearly three years and from MIR to X-ray wavelengths. We present details of our photometric (Section 3) and spectroscopic (Section 4) modelling, motivating our discussion of the potential scenarios of the event (Section 5), after which we conclude by interpreting AT2021lwx as an accretion of a non-stellar, gaseous object onto a large SMBH.

Throughout the paper, we use 'days' to refer to the observer frame and 'd' for the rest frame at z = 0.9945. All photometry is corrected for Galactic foreground extinction according to Schlafly & Finkbeiner (2011) assuming a Fitzpatrick (1999) extinction curve. Magnitudes are presented in the AB system (Oke & Gunn 1983). Upper limits and uncertainties are at the 1σ level. Where necessary we assume a spatially flat lambda cold dark matter cosmological model with H_0 = 70 km s^{-1} Mpc^{-1} and Ω_M = 0.3.

Table 1. Summary of the multiwavelength observations of AT2021lwx.

MJD	Epoch (rest frame d)	Instrument	Bands
		Photometry	
58750 to 59937	−271 to +323	ZTF	g, r
58113 to 59908	−590 to +309	ATLAS	c, o
56803 to 59966 ,	−1247 to +114,	WISE	$W1, W2$
59923, 59966	+317, +338	*Swift* UVOT	$uvw2, uvm2, uvw1, u, b, v$
		X-ray	
59923, 59966	+317, +338	*Swift* XRT	0.3 – 10 keV
		Spectroscopy	
59345, 59844	+27, +277	NTT EFOSC2	3685 – 9315 Å
59931	+320	GTC EMIR	0.85 – 1.35 μm
59949	+329	GTC EMIR	1.45 – 2.42 μm

2 OBSERVATIONS

AT2021lwx was discovered as a transient in Zwicky Transient Facility (ZTF; Bellm et al. 2019; Graham et al. 2019) imaging on the 13th of April 2021. Forced photometry revealed it to have been brightening since at least 16th June 2020 as ZTF20abrbeie. It was independently detected by the Asteroid Terrestrial-impact Last Alert System (ATLAS; Tonry et al. 2018; Smith et al. 2020) as ATLAS20bkdj and the Panoramic Survey Telescope and Rapid Response System (Pan-STARRS; Wainscoat et al. 2016; Chambers et al. 2016) as PS22iin. AT2021lwx was twice observed by the extended Public ESO Spectroscopic Survey for Transient Objects 'plus' (ePESSTO+; Smartt et al. 2015) and was classified as an AGN at z = 0.995 (Grayling et al. 2022). In this section we describe photometric observations of AT2021lwx at X-ray, ultraviolet, optical, near- and mid-infrared wavelengths, which are summarised in Figure 1. Times t are given in the rest frame at z = 0.9945 with respect to maximum light, which we take as the date of the brightest r-band observation: MJD 59291.

2.1 Optical photometry

The optical light curve is compiled using photometry from publicly available ZTF g- and r-band photometry[1], which we obtained via the ZTF forced photometry service (Masci et al. 2019). In addition, we obtained ATLAS c ("cyan", 4200 – 6500 Å) and o ("orange", 5600 – 8200 Å) imaging over the course of the light curve. The region was also covered infrequently as part of the ongoing Pan-STARRS Near Earth Object search which provides $grizy$ coverage.

[1] https://lasair-ztf.lsst.ac.uk/object/ZTF20abrbeie/

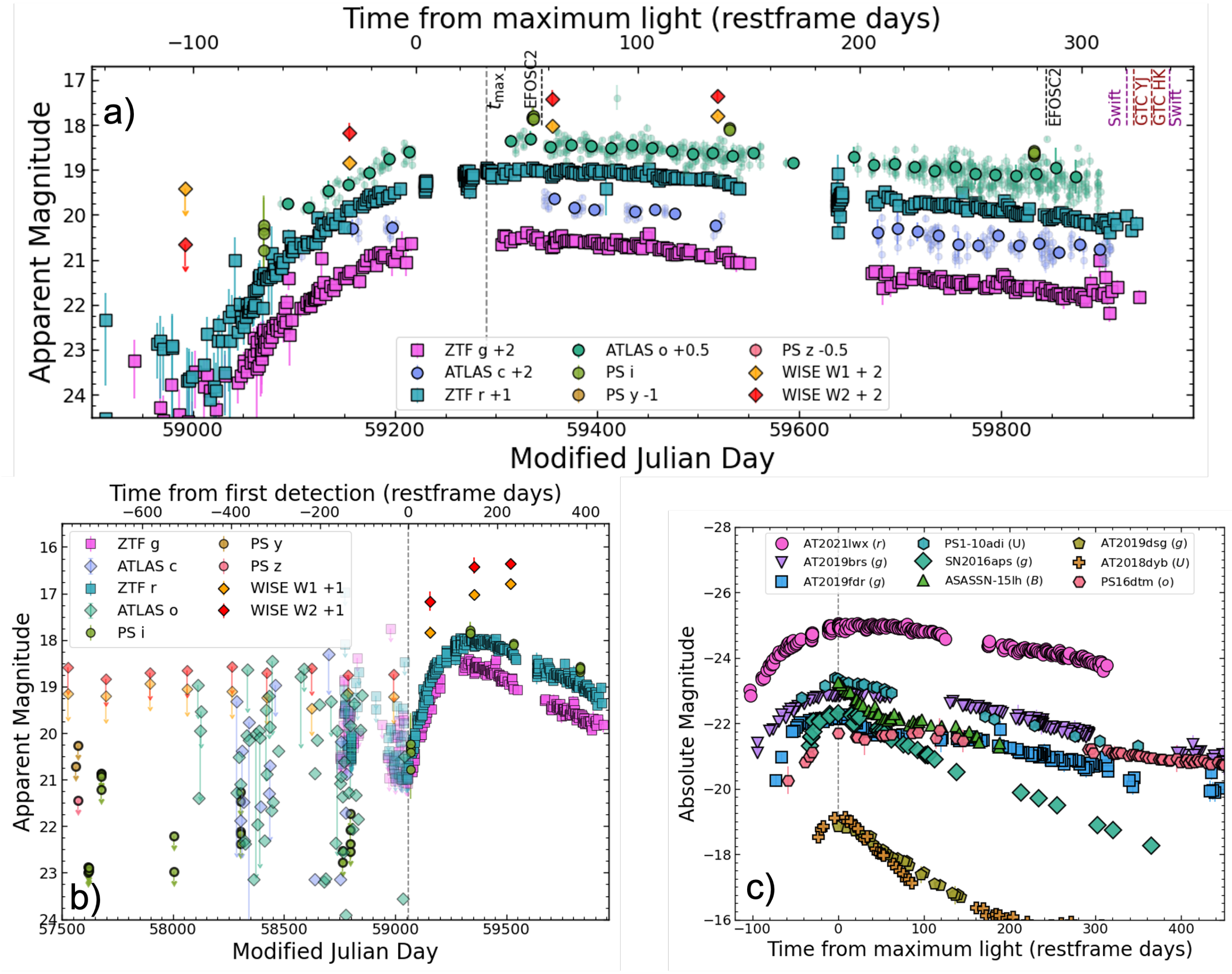

Figure 1. a) Light curve of AT2021lwx. Epochs of our multiwavelength follow-up observations are marked with dashed lines; b) Pan-STARRS upper limits up to 750 d (rest frame) before the first detection of AT2021lwx; c) Comparison to similar transients: NLSy1 accretion events AT2019fdr and AT20219brs (Frederick et al. 2021) and the prototype nuclear flare PS1-10adi (Kankare et al. 2017); the most luminous known likely TDE ASASSN-15lh (Leloudas et al. 2016); the most luminous known supernova SN2016aps (Nicholl et al. 2020); a likely jetted TDE AT2019dsg (van Velzen et al. 2021), a typical TDE AT2018dyb (Leloudas et al. 2019), and the MIR-brightening TDE PS16dtm (Petrushevska et al. 2023)

Data from both ATLAS and Pan-STARRS were obtained as forced photometry[2] (Smith et al. 2020).

To search for a host galaxy, we use the stacked *grizy* images from the Pan-STARRS 3π survey (Waters et al. 2020). We use the `photutils` package and perform photometry in a circular aperture with a 1″ radius centered on the location of AT2021lwx, and use the PS1 weight image to estimate the photometric uncertainties.

2.2 Mid-infrared photometry

The location of AT2021lwx was observed by the Wide-field Infrared Survey Explorer (WISE) spacecraft as part of the NEOWISE reactivation mission (Mainzer et al. 2011). We obtained NEOWISE photometry in the $W1$ and $W2$ bands from the NASA/IPAC infrared science archive[3]. Observations of the location exist with a six month cadence from several years before the flare until November 2021, during its decline. In particular we highlight MJDs 58993 (pre-flare), 59156 (on the rise), 59357 (around peak), and 59520 (during the decline). For each epoch, we use the IRSA WISE/NEOWISE coadder (Masci & Fowler 2009) to combine individual frames. We use a sigma-clipped median to estimate the background, which we subtract and perform aperture photometry in a 4″ radius around the transient location, corresponding roughly to the point spread function of WISE. Before the optical transient, we find no significant detection; after the optical flare begins there is a clear point source in both $W1$ and $W2$.

[2] https://fallingstar-data.com/forcedphot/

[3] https://irsa.ipac.caltech.edu/Missions/wise.html

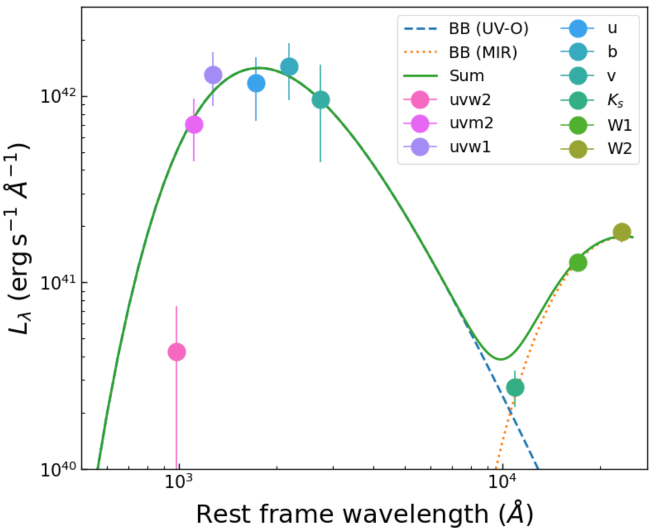

Figure 2. The rest frame UV to MIR SED of AT2021lwx at +338 d. The MIR data come from +114 d and are not scaled as we do not predict their evolution. Data are corrected for MW reddening, but not for any host extinction. The uvw2 point is not included in the black body fit due to likely Lyman-α absorption.

2.3 X-ray and ultraviolet observations

We obtained two epochs of observations with the Neil Gehrels Swift Observatory (*Swift*; Gehrels et al. 2004). The first observation took place at MJD 59923.554 ($t_{\rm max}$ +317 d), and lasted 2670 s. The second took place at MJD 59966.483 ($t_{\rm max}$ + 338 d) and lasted 2605 s. Data were observed in photon counting mode with the X-ray Telescope (XRT; Burrows et al. 2005), and in the *uvw*2 (central wavelength, 1928 Å), *uvm*2 (2246 Å), *uvw*1 (2600 Å), *u* (3465 Å), *b* (4392 Å) and *v* (5468 Å) filters with the Ultraviolet-Optical Telescope (UVOT; Roming et al. 2005), respectively.

The XRT data were reduced with the tasks XRTPIPELINE and XSELECT. The source and background events were extracted using a circular region of 40″ and an annular ring with inner and outer radii of 60″ and 110″, respectively, both centered at the position of the source. The Ancillary Response Files (ARFs) were created with the task XRTMKARF and the Response Matrix File (RMF), swxpc0to12s6_20130101v014.rmf, was taken from the Calibration Data base[4]. Due to the low count rates, the XRT spectra were grouped to have a minimum of 3 counts per bin using the FTOOL GRPPHA.

In terms of the UVOT data, we used the task UVOTIMSUM to sum all the exposures when more than one snapshot was included in each individual filter data and the task UVOTSOURCE to extract magnitudes from aperture photometry. A circular region of 5″ centered at the target position was chosen for the source event and another region of 40″ located at a nearby position was used to estimate the background emission.

2.4 Optical spectroscopy

Optical spectra were obtained on MJD 59345 and MJD 59844 ($t_{\rm max}$ + 27 d and $t_{\rm max}$ + 277 d respectively) via the European Southern Observatory (ESO) as part of ePESSTO+ using the ESO Faint Object Spectrograph and Camera (EFOSC2; Buzzoni et al. 1984) on the New Technology Telescope (NTT) at ESO La Silla observatory, Chile. The first epoch consisted of a single 600 s exposure, while the second epoch consisted of two 2700 s exposures. All three spectra made use of grism13 (3685 – 9315 Å, resolution ~ 17 Å). These spectra were reduced using the PESSTO pipeline (Smartt et al. 2015) v3.0.1.

2.5 Near infra-red spectroscopy

We observed AT2021lwx on MJD 59931 and MJD 59949 ($t_{\rm max}$ + 320 d and $t_{\rm max}$ + 329 d respectively) with the Espectrógrafo Multiobjeto Infra-Rojo (EMIR, Balcells et al. 2000) on the 10.8 m Gran Telescopio Canarias (GTC) at Observatorio del Roque de los Muchachos, La Palma, Spain. Spectra were obtained under Director's Discretionary Time proposal GTC05-22BDDT (PI: Müller Bravo) in long-slit mode. The first epoch made use of the *YJ* grism (0.85 – 1.35 μm, resolution ~ 10 Å); the second epoch used the *HK* grism (1.45 – 2.42 μm, resolution ~ 20Å).

Both epochs used a 1.0" slit. Image rectification, dark and flat fielding, sky subtraction, dither combination, and wavelength calibration were performed using `PyEMIR` (Pascual et al. 2010; Cardiel et al. 2019) v0.17. Cosmic rays were detected and removed using the `lacosmic` algorithm (van Dokkum 2001). Trace extraction was performed manually using `python`. Telluric features were removed by observing and subtracting the spectrum of the telluric standard star HIP104599.

3 PHOTOMETRIC PROPERTIES

The light curve of AT2021lwx (Fig. 1a) peaked in the observer-frame r-band on MJD 59291, 122 d after and 3 mag brighter than the first ZTF detection. The decay tends to a smooth decline of ~ 0.004 mag d^{-1}, consistent with an exponential ($e^{-0.005t}$) decay, while the late time decline is also consistent with the power-law $t^{-5/3}$. To measure the (pseudo-) bolometric light curve we K-correct the observed magnitudes according to Hogg et al. (2002) by assuming a black body as the underlying spectral energy distribution (SED). By correcting the observed r-band to the rest-frame u we are able to compare to similar events at lower redshift. For those objects for which rest-frame light curves are not public, we estimate a K−correction to the u-band by choosing the observer frame band that is closest to u when shifted to the rest frame. We then add the correction of $-\log(1+z)$ to account for the shortening of the wavelength range of the emission in the rest frame. The rest-frame UV peak absolute magnitude is $M \sim -25.7$ mag.

3.1 Comparison to similar events

We build a comparison sample by selecting the most luminous examples of transients from a variety of observational classes, the rest frame u-band absolute magnitude light curves of which we show in Fig. 1b. Our choice of objects serves two purposes: first, we search the literature for the brightest known objects of various classes; second, we show typical examples of TDEs, the most likely candidate for the type of event that could produce such extreme luminosity.

The light curve and luminosity of AT2021lwx most closely resemble a handful of transients detected in known narrow-line Seyfert 1 (NLSy1) galaxies presented by Frederick et al. (2021), from which we select the two that display the brightest luminosity and longest

[4] `https://heasarc.gsfc.nasa.gov/docs/heasarc/caldb/swift`

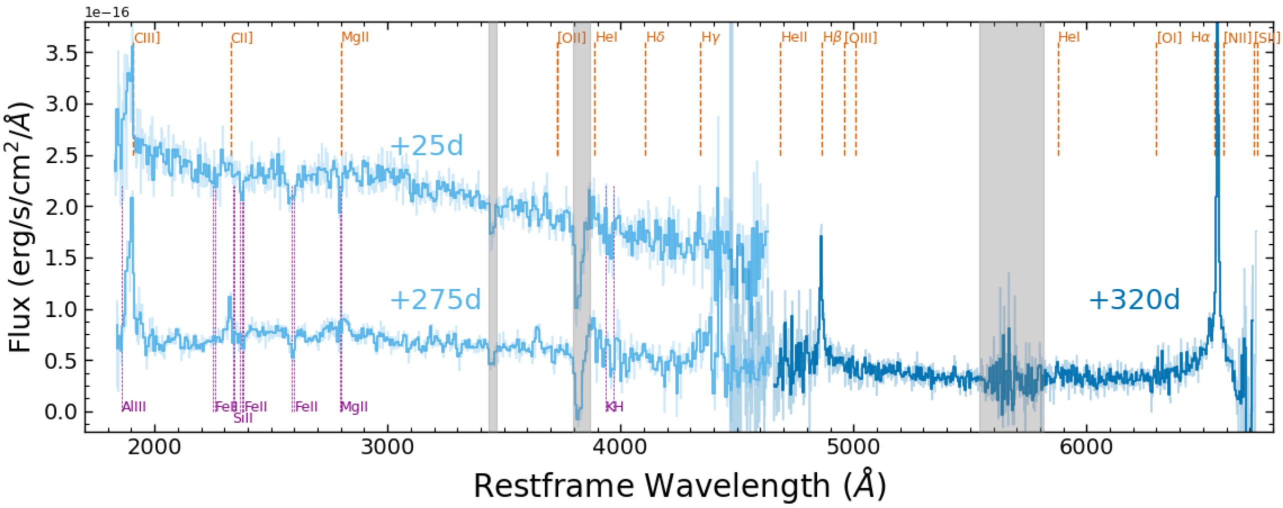

Figure 3. Rest frame UV and optical spectra of AT2021lwx. For clarity, the GTC EMIR +320 d spectrum (dark blue) has been scaled to match the optical NTT EFOSC2 spectrum from +275 d. Common emission features are shown in gold while absorption features are marked in purple. Telluric absorption has been masked in grey.

timescales, AT2019brs and AT2019fdr. To these we add the even more luminous PS1-10adi (Kankare et al. 2017). NLSy1s are highly accreting AGN, and the flares have been attributed to sudden enhancements of accretion rate (either due to a TDE, or as increased gas flow) onto already-accreting SMBHs. At peak, AT2021lwx is nearly 2.5 times more luminous than any of those events. AT2021lwx is several orders of magnitude brighter than any known supernova (SN; De Cia et al. 2018; Angus et al. 2019; Nicholl et al. 2020). We show the most luminous, SN2016aps (Nicholl et al. 2020), which has been interpreted as a possible pulsational pair instability SN (PPISN). AT2021lwx is ten times more luminous than the extreme TDE ASASSN15-lh (Dong et al. 2016; Leloudas et al. 2016) and three times brighter (in the optical/UV) than the jetted TDE AT2022cmc (e.g. Andreoni et al. 2022; Pasham et al. 2023). We also show three further, more regular TDEs (although the class is diverse; Leloudas et al. 2019; van Velzen et al. 2021): AT2019dsg which likely includes a relativistic jet (van Velzen et al. 2021), the well-studied AT2018dyb (e.g. Leloudas et al. 2019), and the MIR-brightening PS16dtm (e.g. Petrushevska et al. 2023). AT2021lwx is 100 times brighter and decays slower than these TDEs.

3.2 Spectral energy distribution

Using the (K-corrected) UV photometry from $t = 317$ d we fit the spectral energy distribution (SED) with a black body with a Levenberg-Marquardt least squares minimisation. We omit the farthest UV band, uvw2, since there is evidence in the spectrum that a strong Lyman-α absorber is present. The fit is shown in Fig. 2. We measure a black body colour temperature of $T_C = 1.2 \pm 0.1 \times 10^4$ K and radius of $R_{BB} = 1.5 \pm 0.3 \times 10^{16}$ cm, while the $t = 338$ d photometry is best fit by consistent values of ($T_C = 1.3 \pm 0.08 \times 10^4$ K) and ($R_{BB} = 1.3 \pm 0.2 \times 10^{16}$ cm). By integrating the black body spectrum, normalised to the r-band peak brightness, we estimate the maximum pseudo-bolometric luminosity of the transient to be 7×10^{45} erg s^{-1}, which is similar to the median luminosity of quasars (Rakshit et al. 2020). We estimate the total energy radiated by integrating the black body with the simplistic assumption that the SED did not evolve over the duration of the transient. Up until December 2022 (440 rest-frame days from the onset of the event), the transient has radiated 1.5×10^{53} erg. Such a high energy release in a relatively short time is unprecedented for a transient and is usually only associated with continuously accreting SMBHs. Given that the transient becomes redder with time, this assumption likely leads to an underestimate of the peak and total bolometric luminosity.

The XRT observations resulted in the tentative detection of X-rays in the range 0.3−10 keV. Modelling the X-ray spectrum as a power-law, we measure an observed 0.3−10 keV flux of $2.94 \pm 1.59 \times 10^{-13}$ erg s^{-1} cm^{-2}. Correcting for Galactic neutral hydrogen column density 10^{21} cm^{-2} (HI4PI Collaboration, et al. 2016) this flux corresponds to an unabsorbed luminosity of 1.52×10^{45} erg s^{-1}. This luminosity is far higher than expected by extrapolating the UV-optical black body and indicates the presence of a separate emission region. The size of the SMBH inferred from the UV-optical properties precludes the X-rays originating as thermal disk emission, while this X-ray luminosity is of similar order to the UV-optical luminosity at the same epoch. An $L_{\mathrm{optical}}/L_{\mathrm{X-ray}} \sim 1$ is consistent with late-time observations of TDEs (e.g. Gezari et al. 2017; van Velzen et al. 2019; Wevers et al. 2019).

Emission in the MIR is also not consistent with the UV-optical black body. It continues rising after the UV-optical starts to decline, indicative either of reprocessing by dust or from a relativistic jet. Similar effects have been seen in TDEs (e.g. van Velzen et al. 2016; Jiang et al. 2021; Onori et al. 2022; Petrushevska et al. 2023) and are interpreted as the echoes of the UV emission from a dusty 'torus' surrounding the SMBH. From a pseudo-bolometric luminosity of 7×10^{46} erg s^{-1} we follow Jiang et al. (2021) to estimate a sublimation radius of ~ 400 light days. This distance should be reflected in a lag between the UV-optical and MIR emission, but the lack of MIR cadence has so far prohibited laying constraints on the time of peak of the MIR. Again assuming a black body, we measure a colour temperature of $T_C \simeq 10^3$ K and a radius of $R_{BB} \simeq 10^{19}$ cm.

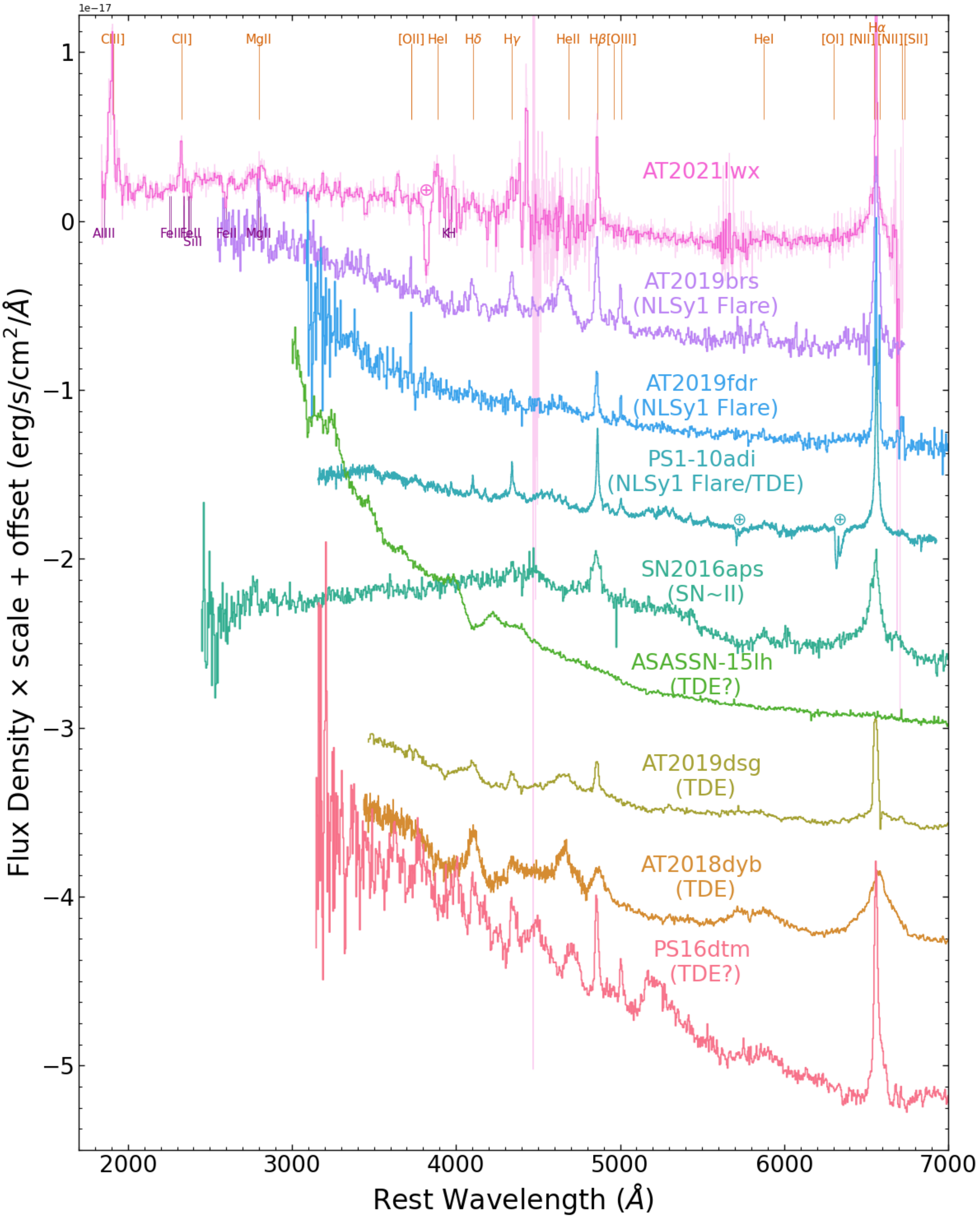

Figure 4. Rest frame UV and optical spectra of AT2021lwx as well as the same objects compared in Fig. 1. Spectra have been shifted and scaled in order to provide a qualitative comparison. Telluric features are marked with ⊕. Spectra have been retrieved from the WISeREP spectral database(Yaron & Gal-Yam 2012).

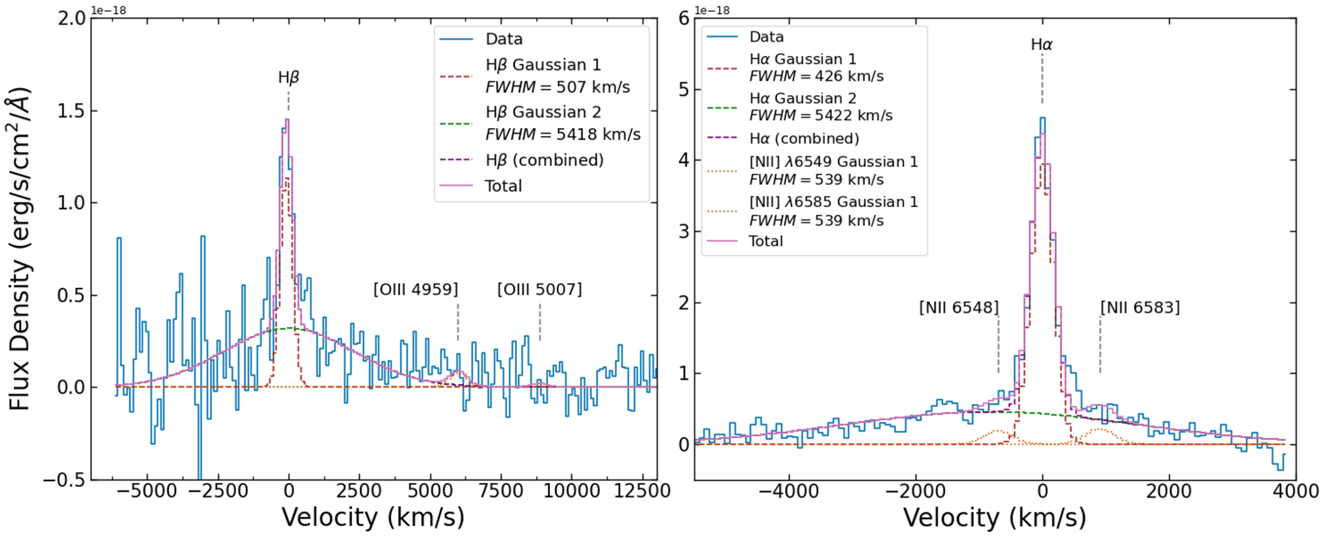

Figure 5. Fits to the Balmer lines Hβ (left) and Hα (right) in the +321 d spectrum. We also show the locations of [O III] and [N II]. The best fit [O III] fluxes are consistent with being caused by noise, while the [N II] lines are marginally significant.

3.3 Host galaxy limits

From the aperture photometry outlined in Section 2.1 we find no significant detections in any band, leading to magnitude limits $g > 23.3$, $r > 23.2$, $i > 23.1$, $z > 22.3$, $y > 21.4$. The i-band limit corresponds roughly to a rest-frame g-band absolute magnitude limit of $M \gtrsim -21.5$ mag. Assuming a mass-to-light ratio $M/L = 2$ results in an stellar mass upper limit of $7{\times}10^{10}\ M_{\odot}$. That is, an average Milky Way-like galaxy would be marginally detected in the imaging. Galaxy stellar mass (M_*) is correlated with the mass of central supermassive black holes. A rough $M_{\rm BH}/M_*$ fraction of 0.025 per cent (Reines & Volonteri 2015) implies a BH of mass $1 \times 10^7\ M_{\odot} \lesssim M_{\rm BH} \lesssim 3 \times 10^8\ M_{\odot}$ for a galaxy with the mass of our estimated upper limit. The PS1 catalogue (Flewelling et al. 2020) contains an object located ∼ 3” northwest of the location of AT2021lwx (PSO 318.4511+27.4315), with $r = 19.25$. If we assume this object is at $z = 0.9945$, then the physical separation is 30.8 kpc, meaning it is unlikely to be associated with the transient. Using the PS1 magnitudes and their uncertainties we estimate a photometric redshift of the nearby object with `EAZY` (Brammer et al. 2008) in its default configuration. We find a best fit photometric redshift $z_{\rm phot} = 2.05 \pm 0.1$, which translates to a restframe UV brightness of −23 mag. This object is either a bright high redshift galaxy, quasar, or a Milky Way star, and is likely unrelated to AT2021lwx.

4 SPECTRAL PROPERTIES

The rest frame UV-optical spectra of AT2021lwx (Fig. 3) are dominated by Balmer emission lines superimposed on a blue continuum which becomes redder with time. Low-ionisation species common to active galactic nuclei (AGN) including Mg II and He I as well as semi-forbidden C III] and C II] are present, but various forbidden nebular lines such as [O II] and [O III] are absent. The spectra are compared to similar objects in Fig. 4 and show similarities and differences to TDEs, SNe and AGN-flares. Particularly noticeable is the absence of lines indicative of Bowen flourescence, which appear to be ubiquitous in AGN flares and are also common in TDEs. Hα and Hβ are well represented by a two-component Gaussian profile (Fig. 5). We fit the two lines both simultaneously (although the fit is dominated by Hα which lies in a much higher signal-to-noise ratio region) and independently. The broad component of Hβ is only marginally detected. To ensure that the broad Hβ component is taken into account, we fix it to the same width as that found from Hα but allow the normalisation to vary freely. The fit results show the lines comprise a narrow component with full-width at half maximum (FWHM) ≃ 430 km s^{-1}, and a broad component with FWHM 5400 km s^{-1}, the broad component being blueshifted by ∼ 500 − 800 km s^{-1}. The width and blueshift are largely dependent on the estimation of the continuum which is affected by the line corresponding to the end of the spectral coverage of the instrument. If the blueshift is confirmed, it indicates outflowing material.

To estimate a reddening we assume Case B recombination for narrow Balmer lines (Osterbrock 1989), with a temperature of $T = 10,000$ K and a density of $n_e = 100\,\mathrm{cm}^{-3}$ and a Calzetti et al. (2000) extinction law (all standard choices for star-forming galaxies; we note that if the narrow Balmer lines are from the transient then Case B may not be appropriate), we measure a modest dust reddening of $E(B-V) = 0.23$. The lack of forbidden oxygen lines in the spectrum allows us to place a limit on the star-formation rate (SFR) of the host galaxy. Correcting the spectrum for Milky Way (MW) and host reddening, we estimate an upper limit on the [O II] luminosity of $5.6{\times}10^{41}$ erg s^{-1}. Using the L([O II]) - SFR relation from Kennicutt (1998), modified according to Kewley et al. (2004), we place an upper limit of SFR $\leq 3.7\,\mathrm{M}_{\odot}\,\mathrm{yr}^{-1}$. Assuming our upper limit on stellar mass of $7 \times 10^{10}\ M_{\odot}$, the SFR - stellar mass relation for average star-forming galaxies at $z = 1$ predicts SFR $\sim 26\,\mathrm{M}_{\odot}\,\mathrm{yr}^{-1}$ (Zahid et al. 2012). We conclude that the host of AT2021lwx is not a highly star-forming galaxy.

The rest-frame UV spectra of AT2021lwx display unresolved absorption features from singly-ionised metal species including Fe II, Mg II and possibly doubly-ionised Al III. The uvw2 luminosity is a factor of 10 smaller than the rest of the UV-optical. In the rest frame

at $z = 0.9945$, uvw2 lies bluewards of Lyman-α. We infer that there is a signifcant Lyman-α absorber located at the systemic redshift, indicating a large reservoir of warm gas, often observed in quasar (e.g. Viegas 1995; Wolfe et al. 2005; Péroux et al. 2006) and gamma-ray burst (e.g. Krühler et al. 2013; Wiseman et al. 2017) spectra.

5 ORIGIN AS AN EXTREME ACCRETION EVENT

AT2021lwx is a highly energetic event, arguably the most luminous optical transient ever observed. Such high luminosity limits the available mechanisms with which to explain the event, which we summarise in this section.

5.1 Tidal disruption event

In this section we discuss the possibility that AT2021lwx is a TDE. We begin by estimating some parameters of the system under the assumption of basic accretion physics and with many simplifications, before discussing the results of two different modelling approaches.

A TDE can only occur when the tidal radius lies outside the event horizon of the black hole. That tidal radius depends upon the density of the star being disrupted such that for a given stellar mass and radius there is a corresponding upper black hole mass limit, the Hills mass (Hills 1975), above which a TDE cannot occur. For a non-rotating black hole, the Hills mass for a typical $1 M_{\odot}$ main-sequence star is $\sim 8 \times 10^{7} M_{\odot}$. Assuming a corresponding radiative efficiency of 0.1 (e.g. Marconi et al. 2004; Alexander & Hickox 2012; Nicholl et al. 2022), the peak luminosity of AT2021lwx corresponds to a mass accretion rate of $\sim 1.2\, M_{\odot}\,\mathrm{yr}^{-1}$. This accretion rate lies at half of the Eddington limit for a black hole of mass $\sim 10^{8}\, M_{\odot}$, which is far larger than the typical black hole mass inferred for TDEs (Mockler et al. 2019; Wevers et al. 2019; van Velzen et al. 2021) and marginally above the Hills mass for a $1 M_{\odot}$ star. Assuming an accretion rate typical of quasars ($\dot{M}/\dot{M}_{\mathrm{edd}} = 0.1$) implies $M_{\mathrm{BH}} \sim 10^{9}\, M_{\odot}$. This is beyond the Hills mass for stars up to $200\, M_{\odot}$ (unless the black hole is rotating with a large spin, in which case the Hills mass increases; Leloudas et al. 2016) and lies close to the mean black hole mass for quasars at $z = 1$ which is $10^{8.5}\, M_{\odot}$ (McLure & Dunlop 2004). Furthermore, at an accretion rate of $1 - 2\, M_{\odot}\,\mathrm{yr}^{-1}$, over two solar masses must already have been accreted, placing that mass as a lower limit on any star to have been disrupted.

The energetics of the event are compatible with a TDE if we expand the range of progenitor stars to far higher masses than have been observed before. Fitting the light curve using Modular Open Source Fitter for Transients (MOSFiT; Guillochon et al. 2018) using the TDE model of Mockler et al. (2019) we estimate $M_{\mathrm{BH}} = 8.3 \times 10^{8}\, M_{\odot}$ and $M_{*} = 14.8\, M_{\odot}$, consistent with accretion close to the Eddington limit. It has previously been assumed that TDEs of such massive stars are extremely rare, not least because the lifetimes of such massive stars are of the order 15 Myr (Meynet & Maeder 2002). A star of this mass must therefore be born within the very central region of the galaxy in order to pass within the tidal radius of the SMBH within its lifetime, which we find unlikely. Similarly, the existence of a $\sim 15\,\mathrm{M}_{\odot}$ star requires strong star formation in the host galaxy which is generally inconsistent with our upper limits. Nevertheless, the MW Galactic centre hosts a population of young ($\lesssim 10-100$ Myr) massive ($\gtrsim 10\, M_{\odot}$) stars, despite there still not being a clear understanding of their origin (e.g. Paumard et al. 2006; Lu et al. 2008). Recent work has also suggested that there are more tidal disruptions of higher-mass stars than previously expected – possible explanations include higher SFR in the centres of these galaxies compared to elsewhere in the galaxies or top-heavy initial mass functions in galactic nuclei producing more higher-mass stars in these regions (Mockler et al. 2022). Furthermore, the apparent overabundance of carbon compared to oxygen is consistent with some observations of evolved asymptotic giant branch stars (e.g. De Beck & Olofsson 2020). Even so, the lower limits from this study were in the $1 - 2\, M_{\odot}$ range, which is far below the mass inferred for AT2021lwx. Furthermore, we note that there is a strong degeneracy in MOSFiT between the radiative efficiency and the stellar mass of the accreted star (Mockler & Ramirez-Ruiz 2021).

It should also be noted that MOSFiT has not been designed to model disruptions of massive stars; it currently only includes zero-age main sequence stars, while a massive star may well be evolved into a more diffuse, giant stage. Indeed, the disruption of evolved stars, or those with diffuse envelopes, is a plausible mechanism for a TDE (e.g. MacLeod et al. 2012; Law-Smith et al. 2017), and while uncertainty in the mass-radius relation from stellar evolution is included in MOSFiT's systematic error measurements, an extreme example could push these errors to the maximum.

Instead of MOSFiT, which relies on simulations of *disruption* and assumes a set of standard relations to describe the transfer of energy from the disrupted material, through the accretion disk, into radiation, we attempt to model the light curve using specific *disk* models that assume an initial disk condition. Following the work of Mummery & Balbus (2020) we are able to explain the peak luminosity and late-time UV-optical SED of AT2021lwx with a $2\, M_{\odot}$ star being disrupted by a higher mass, maximally spinning SMBH of $M_{\mathrm{BH}} > 1 \times 10^{9}\, M_{\odot}$. These results are reliant on a compact initial disc (around the innermost stable circular orbit; ISCO), and a short viscous timescale on the order of the orbital timescale – usually disc timescales are expected to be several orders of magnitude larger than the orbital timescale. We find that including a much larger disc mass (i.e. mass of the disrupted star) drives the temperature to be inconsistent with observations (although this could be rectified if the observations are influenced by significant host galaxy reddening).

Neither of the above models accounts for the possibility of super-Eddington accretion, which is likely to occur in TDEs (Dai et al. 2018), particularly in the early phases of the event. In the super-Eddington regime, the disk is likely to inflate into a geometrically thick disk at which point many of the assumptions used in those models break down. For example, there will be significant mass loss from the disk due to winds, viewing angle effects, and the likely launching of relativistic jets.

The spectra of AT2021lwx do not resemble typical TDEs (e.g. Leloudas et al. 2019; van Velzen et al. 2021; Charalampopoulos et al. 2022). Around half of TDEs appear to show He II, Fe II and/or Bowen features, and while it is fairly common for TDEs to exhibit only Balmer features, such features tend not to include such strong narrow components as AT2021lwx (although see PS16dtm; Petrushevska et al. 2023 and AT2019dsg; van Velzen et al. 2021). If the transient is caused by the disruption of a star, then these spectral features must originate from a reprocessing region not present in typical TDEs. Instead, the narrow components resemble more closely the low-velocity, shocked circumstellar material that gives rise to the narrow lines of type IIn SNe.

Overall, while the light curve, SED and spectra can be explained by a TDE, the nature of such a disruption is highly unconstrained and significant advances in the modelling of both the disruption of massive stars, and the physics of the subsequent accretion, must be made before strong conclusions are drawn.

5.2 Turn on of an AGN via sudden accretion of gas

An alternative to the disruption of a star is the sudden, and isolated, accretion of a large amount of more diffuse material. This is distinct from the classical CLAGN (e.g. LaMassa et al. 2015; Frederick et al. 2019; Graham et al. 2020) which tend to show a change of *spectral* properties. The turn-on scenario has been proposed for the smooth flaring events in known AGN such as AT2017bgt (Trakhtenbrot et al. 2019) and AT2019brs (Frederick et al. 2021). Unlike those transients, there is no evidence for a pre-existing AGN in AT2021lwx, although a low-luminosity AGN is not ruled out due to the larger cosmological distance.

A handful of optical nuclear flares that do not adhere to typical TDE, CLAGN, or SN characteristics have been accumulated over recent years (Kankare et al. 2017; Trakhtenbrot et al. 2019; Frederick et al. 2021). Optically, AT2021lwx is more luminous than all of these events, while the light curve shape is similar to those interpreted as unusual accretion events. Spectroscopically, the two-component Hα profile is similar to the nuclear transient PS1-10adi, with the broad component showing a similar velocity to that transient and AT2017bgt, a long-lasting optical flare in a known AGN. The width of the broad component in AT2021lwx is larger than all other similar nuclear flares in Frederick et al. (2021). Unlike all transients in the comparison sample, the spectrum of AT2021lwx shows no Fe II or features excited by Bowen fluorescence (e.g. N III).

The large widths of the broad lines imply emission from a region with a high-velocity dispersion, while the existence of narrow lines implies a slow-moving component. Such a scenario resembles a traditional AGN according to the unification picture (Antonucci 1993), where broad lines emanate from the eponymous broad-line region (BLR), comprising clouds of gas that follow virialised orbits around a supermassive black hole. If the observed broad Balmer emission originates from an illuminated virialised BLR, then the radius of this region is $r_{\rm BLR} \sim 5 \times 10^{16} - 5 \times 10^{17}$ cm for black holes of $10^8\,M_\odot - 10^9\,M_\odot$ respectively. This inferred BLR size is similar in scale to the inferred black body radius $R_{\rm BB}$, although it is likely that the assumption of a spherical photosphere does not hold if the UV emission originates from an accretion disk.

The narrow line region (NLR) in AGN comprises gas at much larger radii, with light-travel times from black hole to NLR of $10^2 - 10^5$ yr, too far to have been ionised by the current flare of AT2021lwx. If the narrow Balmer lines in the AT2021lwx spectra correspond to a narrow line region in its host galaxy, they must have been ionised by a previously UV-bright source (i.e. an AGN's accretion disk). However, the lack of narrow nebular lines other than from hydrogen and carbon renders the NLR unlikely as the source of these features. A second possible explanation for the lack of [O II], [O III] and narrow Mg II is the Baldwin effect (Baldwin et al. 1977), an observed anti-correlation between AGN luminosity and emission line equivalent widths. Indeed, according to the relationship between B-band absolute magnitude and [O II] equivalent width in Croom et al. (2002) we may not expect to see any [O II] emission at all. [O II] is found to be lacking in around 5 per cent of all AGN (Schawinski et al. 2015).

5.3 Accretion of a gas cloud by a dormant black hole

The lack of evidence for an AGN coupled with the difficulties of explaining the event with a TDE, we explore an alternative origin of AT2021lwx. It is plausible that a large amount of material in the form of a molecular cloud was disrupted (see e.g., Wang et al. 2017) and accreted by the black hole. Assuming a TDE-like scenario, the fuelling rate is determined by the fallback rate of material onto the black hole after the disruption. To achieve the observed rise time, the cloud would need to be compact enough to provide significant fuel at early times, since a diffuse cloud would likely result in a slower fallback rate. Detailed modelling of this scenario is deferred to further work.

5.4 Lensed superluminous supernova

The smooth and slow rise, long decline, and colour evolution of AT2021lwx resemble superluminous SNe (SLSNe), which are thought either to be powered by magnetars (e.g. Woosley 2010; Kasen & Bildsten 2010) or interaction of ejecta with dense circumstellar material (CSM). The latter scenario is particularly likely in the case of SLSNe-IIn (e.g. Smith et al. 2007; Benetti et al. 2014; Nicholl et al. 2020) which display narrow Balmer features as seen in AT2021lwx, raising the possibility of a SN origin for the transient. A number of observed properties deter us from this conclusion. Primarily, the peak luminosity requires an extremely unlikely mass of CSM, of the order 250 $M_\odot$ following Chevalier & Irwin (2011), larger even than the zero-age main sequence mass of the largest expected SN progenitors (e.g. Kasen et al. 2011). The required CSM mass is reduced if the lightcurve is strongly lensed, and thus magnified, by a foreground source. Given the lack of evidence for any galaxy foreground galaxy in deep imaging, nor any system at a lower redshift in the spectra, we find the lensing explanation unlikely.

6 CONCLUSIONS

AT2021lwx is an extraordinary event that does not fit into any common class of transient. With a total radiated energy $> 10^{53}$ erg, it is one of the most luminous transients ever discovered. By collecting and analysing multiwavelength photometry and spectroscopy of the transient, we conclude that:

i) the emission is dominated by a black body with a moderate temperate of 12,000 K and a large radius of 10^{16} cm which cools as the transient fades

ii) there are two components to the material, one with a large velocity dispersion ($\sim$ 5400 km s^{-1}) and another slow-moving component ($\sim$ 430 km s^{-1}), the fast-moving component potentially forming an outflow

iii) the luminosity is likely powered by the accretion of a large amount of gas onto a supermassive black hole with mass $> 10^8$ M$_\odot$

iv) while there is no evidence of AGN activity, there is sign of possibly a hot corona or jet as well as the presence of large amounts of dust

v) a tidal disruption of a massive star is unlikely due to the small chance of such an event observing

vi) the spectral and photometric features of the transient suggest the sudden accretion of a large amount of gas, potentially a giant molecular cloud.

Further follow-up and modelling of AT2021lwx is necessary to reveal more about the scenario that caused the flare, and the community is strongly encouraged to search for similar events in both the future as well as in archival data.

ACKNOWLEDGEMENTS

We thank Nick Stone for helpful discussions on the interpretation of the transient. We are grateful for the rapid turnaround of the DDT proposal by the time allocation committee of the GTC. PW acknowledges support from the Science and Technology Facilities Council (STFC) grant ST/R000506/1. YW acknowledges support from the Royal Society Newton Fund. M.P and G.L. are supported by a research grant (19054) from VILLUM FONDEN. T.E.M.B. acknowledges financial support from the Spanish Ministerio de Ciencia e Innovación (MCIN), the Agencia Estatal de Investigación (AEI) 10.13039/501100011033, and the European Union Next Generation EU/PRTR funds under the 2021 Juan de la Cierva program FJC2021-047124-I and the PID2020-115253GA-I00 HOSTFLOWS project, from Centro Superior de Investigaciones Científicas (CSIC) under the PIE project 20215AT016, and the program Unidad de Excelencia María de Maeztu CEX2020-001058-M. MN is supported by the European Research Council (ERC) under the European Union's Horizon 2020 research and innovation programme (grant agreement No. 948381) and by funding from the UK Space Agency. P.C. acknowledges support via an Academy of Finland grant (340613; P.I. R. Kotak). This work was partially funded by ANID, Millennium Science Initiative, ICN12_009. MG is supported by the EU Horizon 2020 research and innovation programme under grant agreement No 101004719. NI was partially supported by Polish NCN DAINA grant No. 2017/27/L/ST9/03221. This work was supported by a Leverhulme Trust International Professorship grant [number LIP-202-014]. TP acknowledges the financial support from the Slovenian Research Agency (grant P1-0031).

Based on observations collected at the European Organisation for Astronomical Research in the Southern Hemisphere, Chile, as part of ePESSTO+ (the advanced Public ESO Spectroscopic Survey for Transient Objects Survey). ePESSTO+ observations were obtained under ESO program IDs 1103.D-0328, 106.216C and 108.220C (PI: Inserra). Based on observations made with the GTC telescope, in the Spanish Observatorio del Roque de los Muchachos of the Instituto de Astrofísica de Canarias, under Director's Discretionary Time GTC05-22BDDT (PI: Müller Bravo). This work made use of PHOTUTILS (Bradley et al. 2022).

DATA AVAILABILITY

Swift X-ray and UV data are publicly available from the UK Swift Science Data Centre, `https://www.swift.ac.uk/swift_portal`. ZTF data can be retrieved from the ZTF forced photometry service, `https://web.ipac.caltech.edu/staff/fmasci/ztf/forcedphot.pdf`. The GTC spectra will be made public upon acceptance via the GTC archive. WISE data are publicly accessible via the NASA IPAC infra-red science archive (IRSA) at `https://irsa.ipac.caltech.edu`.

REFERENCES

Alexander D. M., Hickox R. C., 2012, New Astron. Rev., 56, 93
Andreoni I., et al., 2022, Nature, 612, 430
Angus C. R., et al., 2019, MNRAS, 487, 2215
Angus C. R., et al., 2022, Nature Astronomy, 6, 1452
Antonucci R., 1993, ARA&A, 31, 473
Arcavi I., et al., 2014, ApJ, 793, 38
Balcells M., et al., 2000, SPIE, 4008, 797
Baldwin J. A., Baldwin A. J., 1977, ApJ, 214, 679
Bellm E. C., et al., 2019, PASP, 131, 018002
Benetti S., et al., 2014, MNRAS, 441, 289
Bradley L., et al., 2022, astropy/photutils: 1.6.0, doi:10.5281/zenodo.7419741, `https://doi.org/10.5281/zenodo.7419741`
Brammer G. B., van Dokkum P. G., Coppi P., 2008, ApJ, 686, 1503
Burrows D. N., et al., 2005, Space Sci. Rev., 120, 165
Buzzoni B., et al., 1984, Msngr, 38, 9
Calzetti D., Armus L., Bohlin R. C., Kinney A. L., Koornneef J., Storchi-Bergmann T., 2000, ApJ, 533, 682
Cardiel N., et al., 2019, ASPC, 523, 317
Chambers K. C., et al., 2016, arXiv, p. arXiv:1612.05560
Charalampopoulos P., et al., 2022, A&A, 659, A34
Chevalier R. A., Irwin C. M., 2011, ApJL, 729, L6
Croom S. M., et al., 2002, MNRAS, 337, 275
Dai L., McKinney J. C., Roth N., Ramirez-Ruiz E., Miller M. C., 2018, ApJ, 859, L20
De Beck E., Olofsson H., 2020, A&A, 642, A20
De Cia A., et al., 2018, ApJ, 860, 100
Dong S., et al., 2016, Sci, 351, 257
Fitzpatrick E. L., 1999, PASP, 111, 63
Flewelling H. A., et al., 2020, ApJS, 251, 7
Frederick S., et al., 2019, ApJ, 883, 31
Frederick S., et al., 2021, ApJ, 920, 56
Gehrels N., et al., 2004, ApJ, 611, 1005
Gezari S., Cenko S. B., Arcavi I., 2017, ApJ, 851, L47
Graham M. J., et al., 2019, PASP, 131, 078001
Graham M. J., et al., 2020, MNRAS, 491, 4925
Grayling M., et al., 2022, TNSAN, 195, 1
Gromadzki M., et al., 2019, A&A, 622, L2
Guillochon J., Nicholl M., Villar V. A., Mockler B., Narayan G., Mandel K. S., Berger E., Williams P. K. G., 2018, ApJS, 236, 6
HI4PI Collaboration, et al., 2016, A&A, 594, A116
Hills J. G., 1975, Nat. 1975 2545498, 254, 295
Hogg D. W., Baldry I. K., Blanton M. R., Eisenstein D. J., 2002, arXiv, pp astro–ph/0210394
Jiang N., et al., 2021, ApJS, 252, 32
Kankare E., et al., 2017, Nat. Astron., 1, 865
Kasen D., Bildsten L., 2010, ApJ, 717, 245
Kasen D., Woosley S. E., Heger A., 2011, ApJ, 734, 102
Kennicutt R. C., 1998, Annu. Rev. Astron. Astrophys., 36, 189
Kewley L. J., Geller M. J., Jansen R. A., 2004, Astron. J., 127, 2002
Komossa S., Grupe D., Komossa S., Grupe D., 2022, arXiv, p. arXiv:2212.10331
Krühler T., et al., 2013, A&A, 557, A18
LaMassa S. M., et al., 2015, ApJ, 800, 144
Law-Smith J., MacLeod M., Guillochon J., Macias P., Ramirez-Ruiz E., 2017, ApJ, 841, 132
Leloudas G., et al., 2016, Nat. Astron., 1, 0002
Leloudas G., et al., 2019, ApJ, 887, 218
Lu J. R., Ghez A. M., Hornstein S. D., Morris M. R., Becklin E. E., Matthews K., 2008, ApJ, 690, 1463
MacLeod M., Guillochon J., Ramirez-Ruiz E., 2012, ApJ, 757, 134
Mainzer A., et al., 2011, ApJ, 731, 53
Marconi A., Risaliti G., Gilli R., Hunt L. K., Maiolino R., Salvati M., 2004, MNRAS, 351, 169
Masci F., Fowler J., 2009, in Bohlender D., Durand D., Dowler P., eds, Astronomical Society of the Pacific Conference Series Vol. 411, Astron. Data Anal. Softw. Syst. XVIII. p. 67 (`arXiv:0812.4310`), doi:10.48550/arXiv.0812.4310
Masci F. J., et al., 2019, PASP, 131, 018003
McHardy I. M., Koerding E., Knigge C., Uttley P., Fender R. P., 2006, Nature, 444, 730
McLure R. J., Dunlop J. S., 2004, MNRAS, 352, 1390
Meynet G., Maeder A., 2002, A&A, 390, 561
Mockler B., Ramirez-Ruiz E., 2021, ApJ, 906, 101
Mockler B., Guillochon J., Ramirez-Ruiz E., 2019, ApJ, 872, 151
Mockler B., Twum A. A., Auchettl K., Dodd S., French K. D., Law-Smith J. A. P., Ramirez-Ruiz E., 2022, ApJ, 924, 70

Mummery A., Balbus S. A., 2020, MNRAS, 492, 5655
Nicholl M., et al., 2020, Nat. Astron., 4, 893
Nicholl M., Lanning D., Ramsden P., Mockler B., Lawrence A., Short P., Ridley E. J., 2022, MNRAS, 515, 5604
Oke J. B., Gunn J. E., 1983, ApJ, 266, 713
Onori F., et al., 2022, MNRAS, 517, 76
Osterbrock D. E., 1989, Astrophysics of gaseous nebulae and active galactic nuclei. http://adsabs.harvard.edu/abs/1989agna.book.....O
Pascual S., Gallego J., Cardiel N., Eliche-Moral M. C., 2010, ASPC, 434, 353
Pasham D. R., et al., 2023, Nat. Astron., 7, 88
Paumard T., et al., 2006, ApJ, 643, 1011
Péroux C., Kulkarni V. P., Meiring J., Ferlet R., Khare P., Lauroesch J. T., Vladilo G., York D. G., 2006, A&A, 450, 53
Petrushevska T., et al., 2023, A&A, 669, A140
Rakshit S., Stalin C. S., Kotilainen J., 2020, ApJS, 249, 17
Reines A. E., Volonteri M., 2015, ApJ, 813, 82
Roming P. W. A., et al., 2005, Space Sci. Rev., 120, 95
Ryu T., Krolik J., Piran T., 2020, ApJ, 904, 73
Scaringi S., et al., 2015, Science Advances, 1, e1500686
Schawinski K., Koss M., Berney S., Sartori L. F., 2015, MNRAS, 451, 2517
Schlafly E. F., Finkbeiner D. P., 2011, ApJ, 737, 103
Smartt S. J., et al., 2015, A&A, 579, A40
Smith N., et al., 2007, ApJ, 666, 1116
Smith K. W., et al., 2020, PASP, 132, 1
Tonry J. L., et al., 2018, PASP, 130
Trakhtenbrot B., et al., 2019, Nat. Astron., 3, 242
Viegas S. M., 1995, MNRAS, 276, 268
Wainscoat R., Chambers K., Lilly E., Weryk R., Chastel S., Denneau L., Micheli M., 2016, Asteroids New Obs. New Model. Proc. Int. Astron. Union, IAU Symp. Vol. 318, pp. 293-298, 318, 293
Wang J. M., Du P., Brotherton M. S., Hu C., Songsheng Y. Y., Li Y. R., Shi Y., Zhang Z. X., 2017, Nat. Astron. 2017 111, 1, 775
Waters C. Z., et al., 2020, ApJS, 251, 4
Wevers T., et al., 2019, MNRAS, 487, 4136
Wiseman P., Schady P., Bolmer J., Krühler T., Yates R. M., Greiner J., Fynbo J. P. U., 2017, A&A, 599, A24
Wolfe A. M., Gawiser E., Prochaska J. X., 2005, Annu. Rev. Astron. Astrophys., 43, 861
Woosley S. E., 2010, ApJ, 719, L204
Yaron O., Gal-Yam A., 2012, PASP, 124, 668
Zahid H. J., Dima G. I., Kewley L. J., Erb D. K., Davé R., 2012, ApJ, 757, 54
van Dokkum P. G., 2001, PASP, 113, 1420
van Velzen S., Mendez A. J., Krolik J. H., Gorjian V., 2016, ApJ, 829, 19
van Velzen S., et al., 2019, ApJ, 872, 198
van Velzen S., et al., 2021, ApJ, 908, 4